JOURNAL OF GEOPHYSICAL RESEARCH, VOL. 102, NO. C2, PAGES 3255–3266, FEBRUARY 15, 1997

Response of global upper ocean temperature to changing solar irradiance

Warren B. White
Scripps Institution of Oceanography, University of California at San Diego, La Jolla

Judith Lean
Naval Research Laboratory, E. O. Hulburt Center for Space Research, Washington, D. C.

Daniel R. Cayan[1] and Michael D. Dettinger
U.S. Geological Survey, San Diego, California

Abstract. By focusing on time sequences of basin-average and global-average upper ocean temperature (i.e., from 40°S to 60°N) we find temperatures responding to changing solar irradiance in three separate frequency bands with periods of >100 years, 18–25 years, and 9–13 years. Moreover, we find them in two different data sets, that is, surface marine weather observations from 1990 to 1991 and bathythermograph (BT) upper ocean temperature profiles from 1955 to 1994. Band-passing basin-average temperature records find each frequency component in phase across the Indian, Pacific, and Atlantic Oceans, yielding global-average records with maximum amplitudes of 0.04° ± 0.01°K and 0.07° ± 0.01°K on decadal and interdecadal scales, respectively. These achieve maximum correlation with solar irradiance records (i.e., with maximum amplitude 0.5 W m^{-2} at the top of the atmosphere) at phase lags ranging from 30° to 50°. From the BT data set, solar signals in global-average temperature penetrate to 80–160 m, confined to the upper layer above the main pycnocline. Operating a global-average heat budget for the upper ocean yields sea surface temperature responses of 0.01°–0.03°K and 0.02°–0.05°K on decadal and interdecadal scales, respectively, from the 0.1 W m^{-2} penetration of solar irradiance to the sea surface. Since this is of the same order as that observed (i.e., 0.04°–0.07°K), we can infer that anomalous heat from changing solar irradiance is stored in the upper layer of the ocean.

1. Introduction

Solar-related decadal and interdecadal changes are ubiquitous in climate records of land and sea surface temperatures [e.g., *Newell et al.*, 1989; *Allen and Smith*, 1994; *Mann and Park*, 1994], U.S. drought [e.g., *Mitchell et al.*, 1979], rainfall [e.g., *Currie and O'Brien*, 1988; *Seleshi et al.*, 1994; *Perry*, 1994], forest fires [e.g., *Auclair*, 1992], and cyclones [e.g., *Cohen and Sweester*, 1979]. However, the limited geographical coverage of most of these records renders them unreliable indicators for solar-related climate change. Indeed, even when climate records with global distribution are available, such as the gridded land and sea surface temperature anomalies compiled at the University of East Anglia [*Parker et al.*, 1994], analyses designed to detect solar-related decadal and interdecadal climate change yield inconsistent results. *Allen and Smith* [1994] analyzed this data set with Monte Carlo singular-spectrum analysis, finding no significant interdecadal signals and significant decadal signals only in the equatorial Atlantic Ocean. *Mann and Park* [1994] analyzed this data set with singular value decomposition, finding significant decadal and interdecadal signals only over northern hemisphere continents. *Dettinger et al.* [1995] analyzed the portion of this data set over the United States, finding no evidence for solar-related decadal or interdecadal signals. On the other hand, *Lau and Weng* [1995] applied wavelet transform analysis to the global-average northern hemisphere portion of this data set, finding significant solar-related signals on both decadal and interdecadal scales.

We inquire into the global connection between decadal and interdecadal climate variability and changing solar irradiance by focusing upon the oceanic portion of the global surface temperature record from 1990 to 1991. We complement it with a new global upper ocean temperature record compiled mostly from bathythermograph (BT) measurements collected from 1955 to 1994. The latter allows us to examine the heat budget of the oceanic response to changing solar irradiance in a simple way not possible over land, answering the question, Where is the anomalous heat from changing solar irradiance stored? By taking this approach we are able to achieve complementary specifications of solar-related decadal and interdecadal signals in upper ocean temperature in these two independent data sets (and in three independent ocean basins). Three different statistical techniques (i.e., power spectra, multichannel singular spectrum analysis (MSSA), and empirical orthogonal function (EOF)) are used to show significant associations between global-average upper ocean temperature and solar irradiance on both decadal and interdecadal timescales. These yield estimates for phase lags of the global-average sea surface temper-

[1]Also at Scripps Institution of Oceanography, University of California at San Diego, La Jolla.

Paper number 96JC03549.
0148-0027/97/96JC-03549$09.00

ature response to changing solar irradiance and estimates for depths to which the temperature response penetrates into the upper ocean on both timescales. These two pieces of information (i.e., phase lags and penetration depths) allow an anomalous global-average heat budget to be constructed for the upper ocean temperature response to changing solar irradiance at the sea surface (i.e., solar insolation), yielding amplitudes for the responses and phase lags that are of the same order as those observed.

2. Observations and Methods

Two independent, but complementary, ocean temperature data sets are employed. They are the Global Ice and Sea Surface Temperature (GISST) sea surface temperatures extending from 1900 to 1991 [*Folland and Powell*, 1994] and the bathythermograph (BT) temperatures extended from 1955 to 1994 [*White*, 1995]. GISST data derive from surface marine weather observations which have undergone considerable quality control, with random errors reduced to approximately ±0.5°K through interpolation onto a 1° latitude-longitude grid each month. BT data derive from vertical temperature profiles from mostly mechanical, digital, and expendable bathythermographs extending from the sea surface to at least 160 m depth. They have undergone considerable quality control, with random errors reduced to approximately ±0.4°K through optimum interpolation [*Gandin*, 1963] onto a 2° latitude by 5° longitude grid at depths of 0, 20, 40, 60, 80, 120, and 160 m each month. Subsequently, for both GISST and BT temperature-gridded fields, gaps in the time record were filled by applying maximum-entropy spectral analysis to each individual time series [*Andersen*, 1974]. Where gaps exceeded 20% of the record, time sequences were eliminated from further consideration. This yielded complete records for GISST data from 40°S to 60°N for 92 years from 1900 to 1991. It yielded complete records for BT data from approximately 30°S to 60°N for 40 years from 1955 to 1994.

A major question in this study is whether standard errors of ±0.5°K and ±0.4°K in individual GISST and BT upper ocean temperatures estimates, respectively, can be lowered enough in basin and global averages to resolve expected responses of 0.025°–0.05°K. Errors in area averages decrease from those of individual estimates in proportion to the inverse square root of the number of independent estimates [*Young*, 1962]. Therefore, if we considered each grid point estimate each month to be independent, then errors in basin and global averages would be less than grid point errors by 2–3 orders of magnitude. However, *White* [1995] determined that individual grid point estimates of upper ocean temperature variability are not independent, with anomalous variability dominated by decorrelation scales ranging from 3 to 6 months, 2.5°–5° latitude, and 5°–10° longitude, smaller in the Atlantic and Indian Oceans than in the Pacific Ocean. As such, we estimate here that approximately 90, 50, and 30 independent estimates occur in the Pacific, Atlantic, and Indian Oceans, respectively, every 3 months. This yields a conservative estimate for standard errors in basin-average monthly mean temperatures, ranging from ±0.04° to 0.08°K in both data sets. These errors are subsequently reduced by approximately 4 (i.e., ±0.01°–0.02°K) when computing band-passed anomalies that detect decadal signals (i.e., assuming four independent estimates per year) and by approximately 6 (i.e., to ±0.007°–0.014°K) when computing band-passed anomalies that detect interdecadal signals. Errors in the global average are reduced from basin-average errors by nearly another factor of 2, reducing largest standard errors to ±0.01°K.

For information about solar irradiance changes over the past century, and in lieu of the commonly used but geophysically irrelevant sunspot number, we utilize reconstructed solar irradiance based on a statistical model calibrated with space-based measurements of solar radiative output over the past 15 years [*Lean et al.*, 1995a]. Estimates outside this time base are available from reconstructions based on knowledge of sources of irradiance variability deduced from extant radiometry, extended in time using parameterizations with appropriate solar activity proxies. The 11-year solar irradiance cycle occurs because bright solar faculae and dark sunspots modulate the Sun's radiation. The irradiance has been reconstructed since 1874 from calculations of sunspot darkening derived from information about sunspot areas and disk positions obtained from ground-based white-light solar images. Facular brightening associated with the solar activity cycle is derived from observations by the Active Cavity Radiometer Irradiance Monitor (ACRIM) on the Solar Maximum Mission Satellite [*Wilson and Hudson*, 1991] by correlating monthly mean values of measured irradiance corrected for sunspot darkening (called the residual irradiance) with monthly mean sunspot numbers (following *Foukal and Lean* [1990]). Estimates of global-average values at the sea surface (i.e., solar insolation) are smaller than irradiance values at the top of the atmosphere by a factor of 4 (i.e., due to averaging over the globe) and by an additional factor of 30% due to reflections associated with cloud and surface albedos [*Wigley and Raper*, 1990; *Reid*, 1991].

A major question impacting this study is whether changing solar irradiance influences global-average upper ocean temperature directly through solar insolation or whether it influences it indirectly through its impact upon the intervening atmospheric wind and cloud patterns. *Haigh* [1996] examined the influence of the ultraviolet (UV) portion of changing solar irradiance upon stratospheric ozone in an atmospheric general circulation model, finding subsequent heating altering stratospheric and tropospheric winds, displacing them poleward during peak solar irradiance. H. Svensmark and E. Friis-Christensen (Variation of cosmic ray flux and global cloud coverage—A missing link in solar-climate relationships, submitted to *Journal of Atmospheric and Terrestrial Physics*, 1996) (hereinafter referred to as Svensmark and Friis-Christensen, submitted manuscript, 1996) examined the influence of changing solar irradiance upon cosmic ray activity (i.e., responsible for ionization in the troposphere), finding it modulating global cloud cover, decreasing it during peak solar irradiance. While we cannot establish in this study whether these atmospheric influences are responsible for some portion of the upper ocean temperature response to changing solar irradiation, *Lean et al.* [1995a] have determined that during the 11-year-cycle, the total irradiation at UV 200–300 nm contributes only about 12% of the total irradiance change. From the Maunder Minimum to the present, the UV 200- to 300-nm radiation is estimated to contribute even less, that is, about 6% of the total irradiance change [*Lean et al.*, 1995b]. These differences in long-term and 11-year UV components of total irradiance variability reflect different competing roles of sunspot darkening and facular brightening estimated to be influencing the Sun's radiative output on different timescales. Regardless, approximately 90% of the total irradiance change on decadal and interdecadal timescales is at wavelengths that penetrate to the

troposphere, allowing direct forcing of sea surface temperature by the changing solar insolation to be a plausible mechanism.

3. Global Upper Ocean Temperature and Solar Irradiance Anomalies

By way of introduction, we compute global-average sea surface temperature anomalies from both GISST and BT data sets for the overlapping 38-year period from 1955 to 1991. Area averages extend from 40°S to 60°N for the GISST data set and from approximately 30°S to 60°N for the BT data set, weighted toward the tropics by the cosine of latitude. Subsequently, each time sequence is low-pass-filtered to suppress interannual variability with a half-power point at 7 years [*Kaylor*, 1977], yielding time sequences that reveal decadal and interdecadal variability remarkably similar to that observed in the corresponding time sequence of reconstructed solar irradiance (Figure 1). All three low-passed time sequences display peak anomalies near 1960, 1970, 1980, and 1990, consistent with decadal signals observed by *Allen and Smith* [1994] and *Lau and Weng* [1995]. All three time sequences display broad peaks near 1960 and 1985, consistent with interdecadal signals observed by *Mann and Park* [1994] and *Lau and Wang* [1995]. Quantitative estimates of the amplitudes and the relative phasing are determined in the next two subsections by extending the comparison over the longer period (1900–1991), extending it to individual ocean basins, and extending it into the subsurface ocean. Unfiltered BT and GISST records in Figure 1 display global-average variability on interannual scales as well, with peak anomalies occurring during 1958, 1964, 1966, 1969, 1973, 1977, 1980, 1983, and 1988, associated with El Niño in the eastern equatorial Pacific Ocean. These global-average interannual signals have no counterpart in the solar irradiance record.

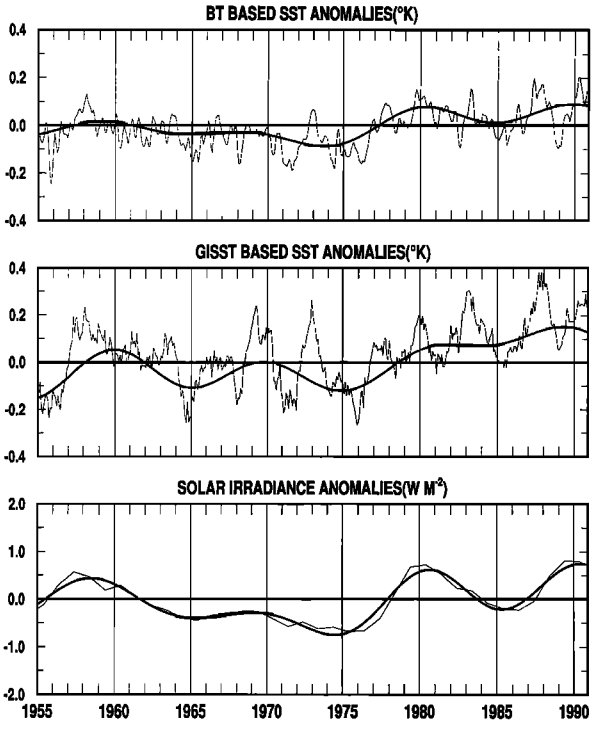

Figure 1. Time sequences of sea surface temperature anomalies (in kelvins) averaged over the global ocean from (middle) GISST and (top) BT data sets from 1955 to 1994. Light curves give individual monthly mean anomalies, and heavy curves give low-pass-filtered versions (i.e., with half-power points at 7 years). (bottom) Time sequences of reconstructed solar irradiance and its corresponding low-pass-filtered version for the same period (in watts per square meter). To avoid loss of data at the ends of each time sequence due to low-pass filtering, maximum-entropy spectral analysis was applied [*Andersen*, 1974] using spectral coefficients to extend both ends of each sequence by half the filter width.

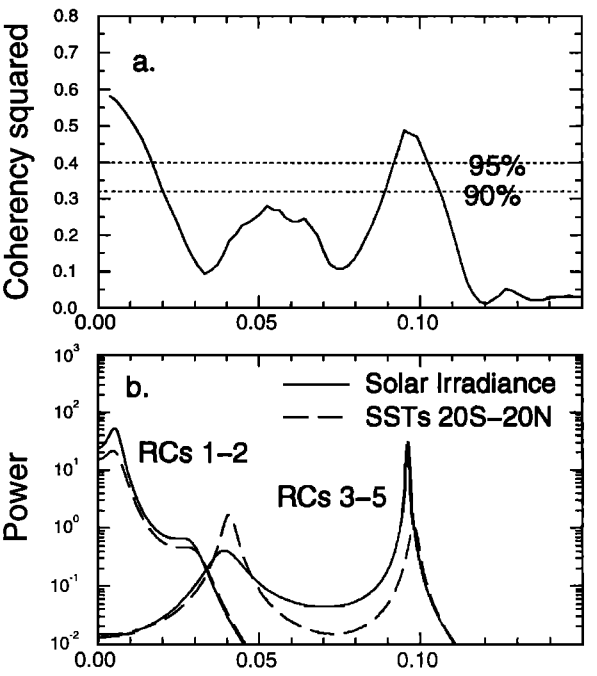

Figure 2. (a) Coherency spectrum for annual time sequences of global, 20°S–20°N, sea surface temperature and solar irradiance anomalies, 1900–1991. (b) Maximum entropy spectrum of leading reconstructed components (RCs) from two-channel singular-spectrum analysis (SSA) of sea surface temperature and solar-irradiance anomalies, with a window width of 27 years. Solar-irradiance fluctuations are at the top of the atmosphere in this and the next figure.

3.1. Cross-Spectrum and Singular-Spectrum Analyses for Associations

To quantify the identification of signals common between global-average sea surface temperature and solar irradiance, their monthly time sequences were analyzed jointly by standard cross-spectrum methods [*Jenkins and Watts*, 1968] and by two-channel singular-spectrum analysis (SSA) [*Vautard et al.*, 1992]. Given the strong periodicities in solar irradiance at nominal 11-year and 22-year periodicities, it is not surprising that both analyses yield shared variations from among this limited set of frequencies.

The coherency spectrum in Figure 2a was computed from a windowed cross periodiogram of the solar irradiance sequence and the global-average tropical (i.e., 20°S–20°N) sea surface temperature sequence from 1900 to 1991 (similar results were obtained from averages between 30°S and 30°N), using a Bartlett-Priestley window function (M = 20 year); confidence limits are from *Granger* [1964]. Coherence at $(9–13 \text{ years})^{-1}$ and at very low frequency exceed the 95% coincidence level. Coherence at $(18–25 \text{ years})^{-1}$ does not quite reach the 90%

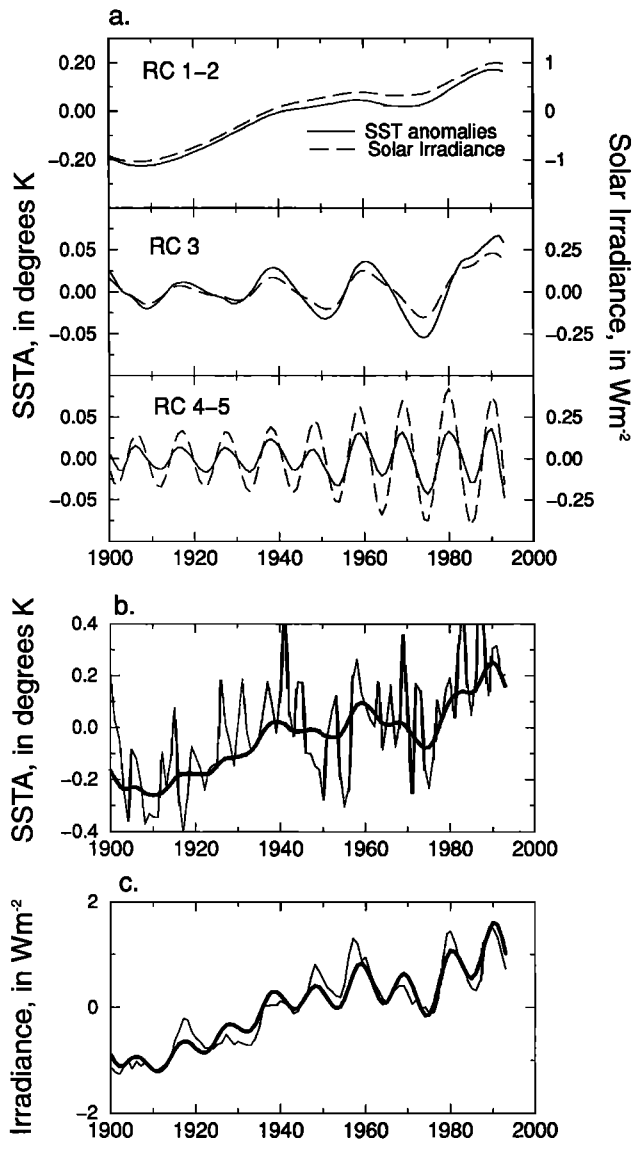

Figure 3. Reconstructed components (RCs) from two-channel SSA of annual global, 20°S–20°N, sea surface temperature and solar-irradiance anomalies, using a window width of 27 years: (a) RCs 1–2, RC 3, and RCs 4–5; (b) RCs 1–6 of sea surface temperature anomalies (heavy curve) and unfiltered anomalies (light curve); and (c) RCs 1–6 of solar irradiance anomalies (heavy curve) with unfiltered anomalies (light curve).

confidence level, but we retain this band because it is also recovered by the SSA of solar irradiance and sea surface temperature. A phase spectrum, corresponding to Figure 2a, was also computed, but wide confidence intervals about the zero phase difference yield uninteresting results on both decadal and interdecadal timescales.

Two-channel singular-spectrum analysis of the two records, using window widths between 20 and 30 years, identifies the same three spectral components, indicated by comparing Figures 2a and 2b. The leading two SSA components capture 36% of the sea surface temperature variance and 69% of the solar-irradiance variance, in the form of very low frequency variations common in both (Figure 2b). These shared low-frequency components are reconstructed in the upper panel of Figure 3b, illustrating the close parallel between solar-irradiance and sea surface temperature trends discussed by *Reid* [1991]. SSA component 3 captures shared interdecadal (i.e., 18- to 25-year period) variability in the two records (Figure 2b and Figure 3a, middle panel), contributed by 2% of the sea surface temperature variance and by 1% of the solar-irradiance variance. Finally, SSA components 4 and 5 capture shared decadal (i.e., 9- to 13-year period) variability in the two records (Figure 3a, lower panel), contributed by 1% of the sea surface temperature variance and by 7% of the solar-irradiance variance. These percentages of variance for decadal and interdecadal signals are small because of preponderance of variance in the trend and the higher frequencies. Significance of SSA components was judged by a screen-plot method [*Vautard et al.*, 1992], typical of principal component analyses. In the plot for the present analysis, the first three components plot well above the noise "floor." Components 4 and 5 plot marginally above the floor, but taken together as "paired eigenvalues" [*Vautard et al.*, 1992], they also appear to be significant. Together, these five components capture coherent signals shared by the time sequences in each of the major low-frequency modes of reconstructed solar irradiance. In contrast, when the solar irradiance time sequence was paired with red noise with the same autoregressive properties as the sea surface temperature time sequence, no such precise pairing of frequencies was found.

3.2. Band-Pass Filtering for Amplitude and Phase Lag Information

Having identified frequencies at which sea surface temperature and solar variations vary coherently, time sequences of low-passed- and band-passed-filtered basin and global averages are calculated to isolate decadal and interdecadal signals. To reveal the decadal signal, BT sea surface temperature anomalies were averaged over the Indian, Pacific, Atlantic, and global oceans from 1955 to 1994 (Figure 4a) together with low-passed versions [*Kaylor*, 1977] computed with a half-power point at 7 years. Area averages extend from 30°S to 60°N, weighted toward the tropics by the cosine of latitude. In each ocean basin and over the global ocean each low-passed record displays fluctuations with peaks near 1960, 1970, 1980, and 1992, with a maximum amplitude of 0.04° ± 0.01°K. These peaks are aligned with those in the nominal 11-year signal in reconstructed solar irradiance (Figure 4a, lower panel), with a maximum amplitude of approximately 0.5 W m^{-2}.

Regression is conducted between band-passed records of global-average sea surface temperature and reconstructed solar irradiance in Figure 4a. The band-pass filter has half-power points at 7 and 15 years [*Kaylor*, 1977], isolating decadal signals from interannual and interdecadal signals in both records as indicated in Figures 2 and 3. Maximum correlation between the two band-passed records is 0.93 ± 0.20 at a 0-year lag, with 95% confidence limits based on Fischer's Z transform [*Snedecor and Cochran*, 1980] using 6° of freedom (i.e., corresponding to the four cycles spanning 1955–1994). These error bars allow phase lags to range from 0 ± 2 years. The corresponding regression coefficient is 0.10 ± 0.02°K (W m^{-2})$^{-1}$, indicating that on average a 0.5 W m^{-2} change in solar irradiance at the top of the atmosphere is associated with a 0.05°K change in global-average sea surface temperature.

To reveal the interdecadal signal, GISST sea surface temperature anomalies were averaged over each ocean basin and over the global ocean from 1900 to 1991 (Figure 4b) together with low-pass versions [*Kaylor*, 1977] computed with a half-

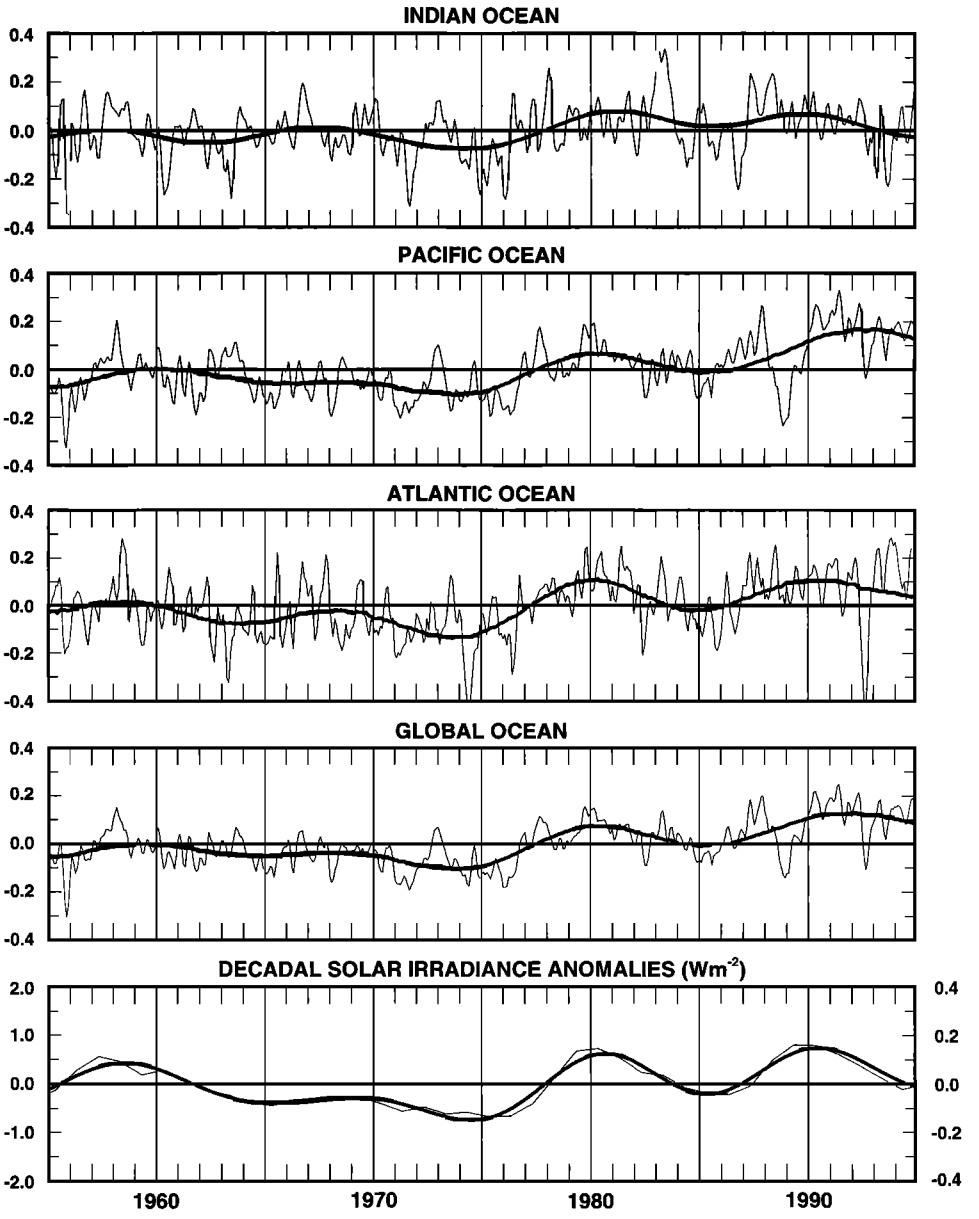

Figure 4a. Time sequences of decadal sea surface temperature anomalies (in kelvins) averaged over Indian, Pacific, Atlantic, and global oceans from the BT data base from 1955 to 1994. Light curves give individual monthly mean anomalies, and heavy curves give low-pass-filtered versions (i.e., with half-power points at 7 years). Also displayed are time sequences of reconstructed solar irradiance and its corresponding low-pass-filtered version for the same period. In the bottom panel, two values of solar irradiance are given; on the left are values at the top of the atmospheres (S_T); on the right are global-average estimates at the sea surface, the solar insolation (i.e., $S = 0.7(S_T/4)$). To avoid loss of at the ends of each time sequence due to low-pass filtering, maximum-entropy spectral analysis was applied [*Andersen*, 1974] using spectral coefficients to extend both ends of each sequence by half the filter width.

power point at 15-year period. In each ocean basin and over the global ocean each low-passed time sequences displays fluctuations with peaks near 1920, 1940, 1960, and 1985, with a maximum amplitude of 0.07° ± 0.01°K, nearly twice that for decadal scales. These peaks are aligned with those in the nominal 22-year cycle of reconstructed solar irradiance (Figure 4b, lower panel), with a maximum amplitude of approximately 0.5 W m^{-2}, similar to that for decadal scales.

Regression is conducted between band-passed records of global-average sea surface temperature and reconstructed solar irradiance in Figure 4b. This band-pass filter has half-power points at 15 and 30 years [*Kaylor*, 1977], isolating interdecadal signals from decadal and longer-term signals in both records as indicated in Figures 2 and 3. Maximum correlation between the two band-passed records is 0.81 ± 0.40 at a 3-year lag, with 95% confidence limits based on Fischer's Z transform [*Snedecor and Cochran*, 1980] using 6° of freedom (i.e., corresponding to the four cycles spanning 1900–1991). These error bars allow phase lags to range from 3 ± 4 years. The corresponding regression coefficient is 0.14 ± 0.02°K $(W\ m^{-2})^{-1}$, indicating that on average a 0.5 W m^{-2} change in solar irradiance at the top of the atmosphere is associated with a 0.07°K change in

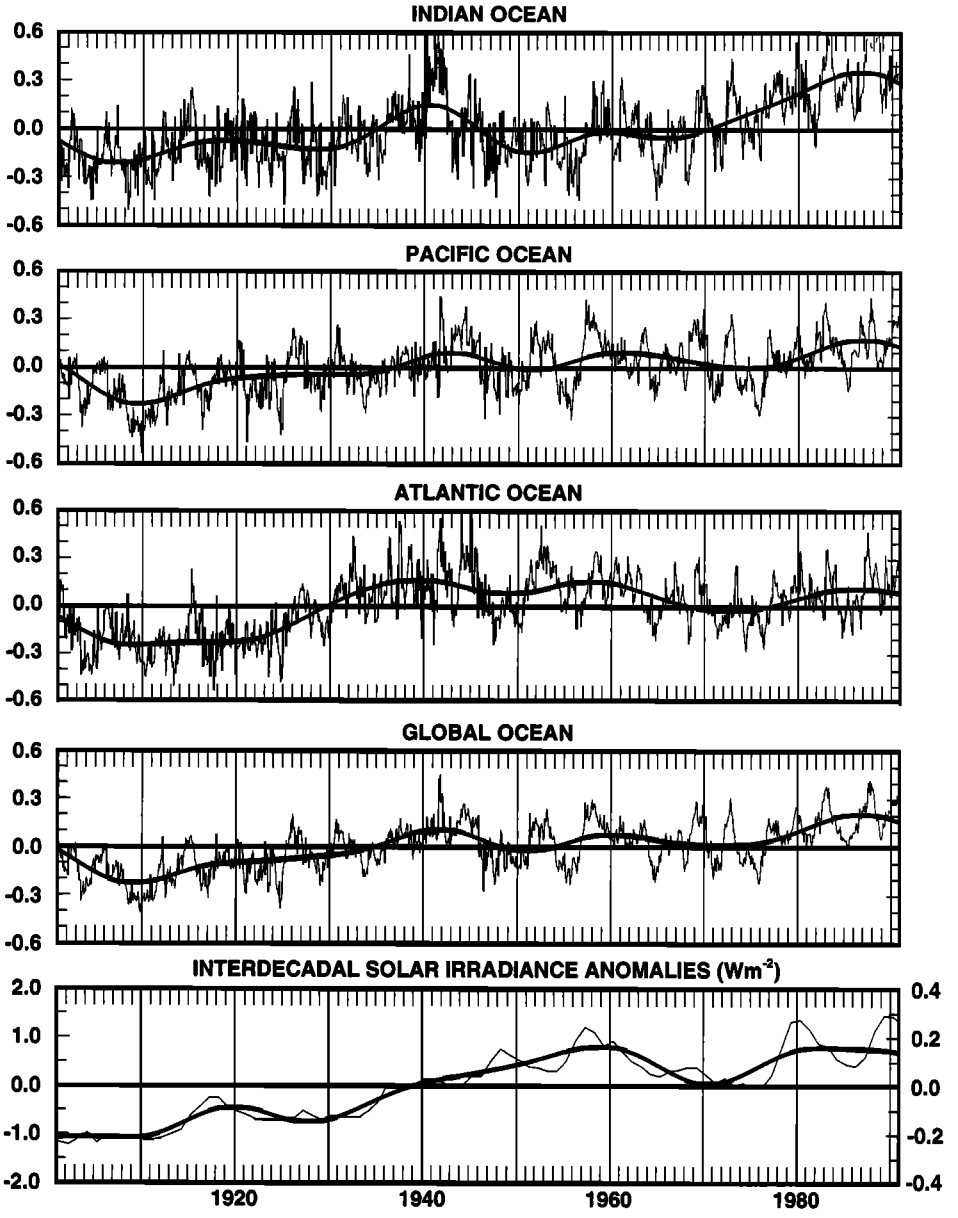

Figure 4b. Same as Figure 4a, but for the interdecadal GISST data set from 1900 to 1991, and with low-pass-filtered versions computed with half-power points at 15 years.

global-average sea surface temperature on interdecedal scales. This is 50% larger than found on decadal scales.

We also use the GISST global-average sea surface temperature record to examine decadal variability from 1900 to 1991. As with the BT record, we apply the band-pass filter with half-power points at 7 and 15 years [*Kaylor*, 1977], isolating decadal signals from interannual and interdecadal signals in both temperature and reconstructed solar irradiance records over this extended period. The GISST band-passed time sequence displays fluctuations with peak anomalies near 1907, 1917, 1928, 1942, 1951, 1961, 1970, 1980, and 1990, again with a maximum amplitude of 0.04°C. Over most of this 92-year record these peaks are aligned with those in the nominal 11-year cycle of reconstructed solar irradiance, with a maximum amplitude of approximately 0.5 W m^{-2}. However, differences occur during the 1940s and early 1950s, with peaks in solar irradiance in 1938 and 1949 leading those in sea surface temperatures by 3–4 years. We suspect that these differences occur because of the disruption in the collection of surface marine weather observations from 1940 to 1945 during World War II (WWII), but this remains to be demonstrated. Even with these differences, maximum correlation between the two band-passed records is 0.65 ± 0.30 at 1-year lag, with 95% confidence limits based on Fischer's Z transform [*Snedecor and Cochran*, 1980], using 16° of freedom (i.e., corresponding to the nine cycles spanning 1900–1991). These error bars allow phase lags to range from 1 ± 2 years. The corresponding regression coefficient is 0.08 ± 0.01°K (W m^{-2})$^{-1}$, indicating that on average a 0.5 W m^{-2} change in solar irradiance at the top of the atmosphere is associated with a 0.04°K change in global-average sea surface temperature on decadal scales. This is nearly the same as observed on decadal timescales for the shorter BT record.

How deep into the ocean do these temperature responses to

changing solar irradiance penetrate? Correlations between decadal and interdecadal global-average BT upper ocean temperature anomalies and corresponding reconstructed solar irradiance anomalies (1955–1994) decrease with depth to insignificance between 80 and 120 m for decadal signals and between 80 and 160 m for interdecadal signals (Figure 5). These penetration depths correspond roughly to the deepest penetration of the global-average near-surface mixed layer [*Robinson*, 1976; *Robinson et al.*, 1979]. They also correspond approximately to the average thickness of the upper layer of the ocean above the main pycnocline. These results, together with a lack of significant lag variation with depth (not shown), indicate that anomalous heat from changing solar irradiance is stored mostly in the upper layer of the ocean on both decadal and interdecadal timescales. It is resisted from penetrating deeper by the stratification of the main pycnocline. Greater penetration seems to have occurred on interdecadal than on decadal scales, but this is somewhat obscured by the reduced statistical significance associated with the longer timescale.

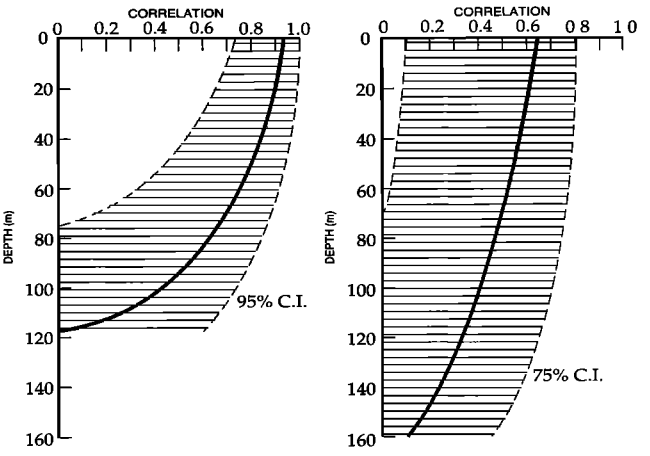

Figure 5. (left) Correlation as a function of depth between global-average BT upper ocean temperature and reconstructed solar irradiance anomalies for 1955–1994 on decadal scales. (right) Correlation as a function of depth between global-average BT upper ocean temperature and solar irradiance anomalies for 1955–1994 on interdecadal scales. Confidence intervals are lined, computed on the basis of Fischer's Z transform [*Snedecor and Cochran*, 1980].

4. Global Patterns of Decadal and Interdecadal Sea Surface Temperature Variability

The dominant empirical orthogonal function (EOF) of decadal BT sea surface temperature anomalies from 1955 to 1994 (Figure 6, upper panel) explains 50% of total variance [*Preisendorfer*, 1988]. The time sequence of this dominant EOF lags the nominal 11-year cycle in solar irradiance by 0–2 years (i.e., 0°–65° of phase). Associated spatial weightings represent the global pattern of decadal sea surface temperature anomalies approximately 1 year after peak solar forcing. This pattern has relatively uniform weightings in tropical portions of the Indian, Pacific, and North Atlantic Oceans, out of phase with those mostly in the western and central extratropical oceans. While global-average sea surface temperature anomalies in Figure 4a display maximum amplitude of 0.04°K, maximum regional amplitude in Figure 6 is 0.15°K (i.e., determined by multiplying maximum weightings in the spatial pattern by maximum amplitude in the corresponding time sequence), 3 times larger than the global average.

The dominant EOF of interdecadal GISST sea surface temperature anomalies from 1900 to 1990 (Figure 6, lower panel) explains 87% of the total variance. The time sequence of this dominant EOF lags the nominal 22-year cycle in solar irradiance by 0–4 years (i.e., 0°–65° of phase). Associated spatial weightings are similar to those for the decadal signal, but more symmetric about the Intertropical Convergence Zone all across the global tropical ocean, with negative weightings in the extratropics displaced farther poleward. This global pattern of sea surface temperature anomalies occurs 2–3 years after peak solar forcing. While global-average sea surface temperature anomalies in Figure 4b achieve a maximum amplitude of 0.07°K, maximum regional amplitude in Figure 6 is 0.3°K, 4 times larger than the global average.

Spatial patterns in Figure 6 have relative uniform weightings over the global tropical ocean, from which most of the global-average sea surface temperature variability in Figures 1–4 derives. In the extratropics, negative weightings tend to cancel positive weightings, so that little contribution to the global-average comes from poleward of 20°–30° latitude. If this holds true for the Southern Ocean (i.e., poleward of 40°S), which is not contained in the current global-average due to lack of observations, then its future inclusion may not significantly alter the results presented here.

5. Global-Average Anomalous Heat Budget of the Upper Ocean

Whether the observed amplitude of global-average upper ocean temperature anomalies can be explained by the observed amplitude of changing solar irradiance is determined by examining the global-average anomalous heat budget [e.g., *Gill*, 1982] for the upper ocean; that is,

$$\partial T/\partial t + KT = S/(\rho C_p H), \tag{1}$$

where T is the vertical- and global-average temperature anomaly, S is the global-average solar irradiance anomaly at the sea surface (i.e., solar insolation anomaly), ρ is the density of sea water, C_p is the specific heat of sea water (4.2×10^3 W s kg^{-1} °K^{-1}), K^{-1} is the dissipation timescale, and H is the depth over which the solar signal in temperature penetrates uniformly into the upper ocean. Since this heat budget represents a global average, advection is assumed to average to zero. In general terms, KT represents global-average anomalous heat loss in the upper ocean to both the atmosphere and the deep ocean. In earlier models, *Hoffert et al.* [1988], *Wigley and Raper* [1990], and *Reid* [1991] interpreted this dissipation as anomalous heat loss to the deep ocean. But results in Figure 5 indicate that this can be neglected on decadal and interdecadal scales, with the upper layer insulated from the deep ocean by the stratification of the main pycnocline. Instead, we interpret KT here to represent the anomalous turbulent-plus-radiative heat loss to the atmosphere.

Representing solar insolation with $S = S_0 \cos(\omega t)$, the solution to (1) is

$$T = [S_0/((\rho C_p H)(K^2 + \sigma^2)^{1/2})] \cos(\omega t - \theta), \tag{2}$$

where ω is the frequency of the solar insolation anomaly and $\theta = \tan^{-1}(\omega/K)$ represents the phase difference between the

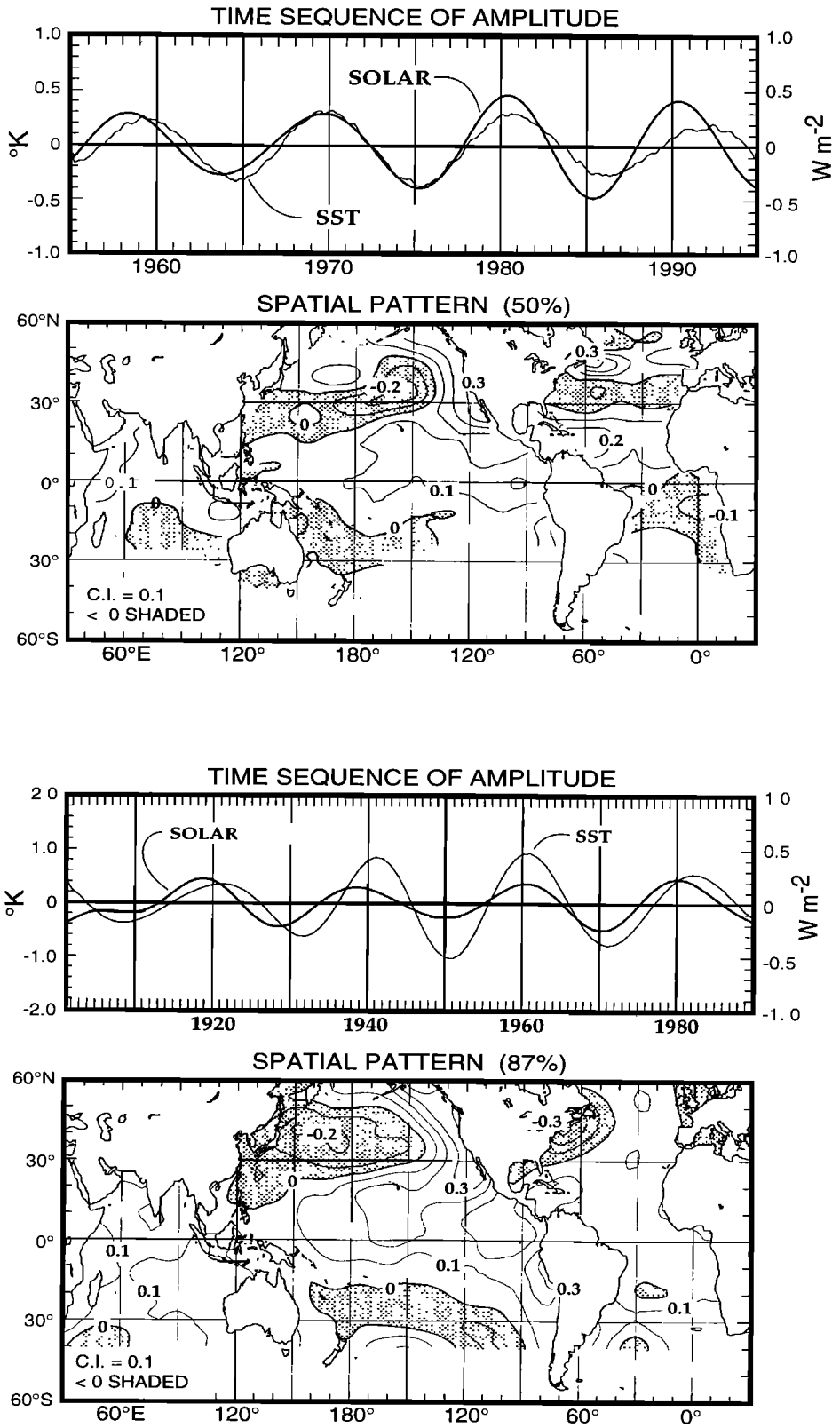

Figure 6. (top) Time sequence and spatial pattern of the first-mode empirical orthogonal function [*Preisendorfer*, 1988] applied to decadal BT sea surface temperature anomalies. This mode, together with its quadrature pair, explains 50% of decadal variance from 1955 to 1994. (bottom) Same as above, but for interdecadal GISST sea surface temperature anomalies, explaining 87% of interdecadal variance from 1901 to 1990. Superimposed on both time sequences are corresponding decadal and interdecadal anomalies of reconstructed solar irradiance anomalies at the top of the atmosphere. In each spatial pattern, negative weightings are shaded, and positive weightings are unshaded.

temperature response and the solar forcing. Knowledge of the phase lag θ from observations allows the dissipation timescale K^{-1} to be estimated, the latter affecting the amplitude of the response. The amplitude of the response is also affected by the depth H over which the solar signal in temperature penetrates uniformly into the upper ocean. Since the correlation between solar irradiance and upper ocean temperature anomalies decreases almost linearly with depth in Figure 5, the depth scale here (i.e., 40–80 m) is taken to be half the deepest penetration observed there (i.e., 80–160 m). In this case, vertically average temperature anomalies in the model become equivalent to sea surface temperature anomalies.

We calculate the amplitude of the global-average sea surface temperature response (T_0) from observed estimates of S_0, K, and H in (2). The amplitude of the solar insolation S_0 is 0.1 W m^{-2} on both decadal and interdecadal scales, 1/5 its maximum amplitude at the top of the atmosphere as explained in the section Observations and Methods. Phase lags θ range from 30° to 50° (i.e., the average of those observed in Figures 4 and 6), corresponding to dissipation timescales K^{-1} of 1–1.5 years on the decadal scales and 2–3 years on interdecadal scales. Depths for the penetration for the responses, H, are 40–60 m on decadal scales and 40–80 m on interdecadal scales, consistent with Figure 5. Therefore, resulting amplitudes of model sea surface temperature responses in (2) are computed to range from 0.01° to 0.03°K on decadal scales and 0.02° to 0.05°K on interdecadal scales, both of the same order as those observed (i.e., 0.04°–0.07°K).

To understand why the global-average sea surface temperature response to changing solar irradiance occurs at phase lags of 30°–50° on average, we examine the ocean's anomalous radiation balance using a modified form for the Stefan-Boltzmann law; that is,

$$\partial S = (4\alpha\sigma T^3)\partial T, \tag{3}$$

where ∂S is global-average solar insolation change, ∂T is the global-average sea surface temperature change, T is the global-average sea surface temperature (i.e., approximately 290°K), σ is the Stefan-Boltzmann constant (i.e., 5.7×10^{-8} W m^{-2} $(°K)^{-4}$), and α is a coefficient (i.e., $(2 - \varepsilon)/2 = 0.61$) representing the influence of the fraction of long-wave back radiation absorbed by the atmosphere (i.e., $\varepsilon = 0.77$) and radiated back into the ocean [*James*, 1994]. Therefore, the 0.1 W m^{-2} amplitude of solar insolation change yields a global-average sea surface temperature change of approximately 0.03°K, of the same order as those observed (i.e., 0.04°–0.07°K).

The anomalous radiation balance assumes that global-average sea surface temperature change comes into balance with changing solar insolation over some equilibration timescale. We can estimate this timescale from consideration of the anomalous heat budget in (1), assuming dissipation KT to be due only to long-wave back radiation. In this case, the inverse equilibration timescale K_E for the upper layer of the ocean of the depth H can be written as

$$K_E = (4\alpha\sigma T^3)/(\rho C_p H). \tag{4}$$

Here, if depth H is taken to be a few meters, then K_E^{-1} would be a few months; if it is taken to be the entire ocean depth, then K_E^{-1} would be decades to centuries. In the present study, with H ranging from 40–60 m on decadal scales and 40–80 m on interdecadal scales, (4) yields K_E^{-1} ranging from 1.6 to 2.4 years on decadal scales and 1.6 to 3.2 years on interdecadal scales. For the anomalous heat budget model in (1) to be consistent with the anomalous radiation balance in (3) these estimates for K_E^{-1} set the upper limit for K^{-1} in the model. They also set upper limits for model phase lags, approximately 50°–75° on decadal scales and 40°–50° on interdecadal scales, similar to those observed (i.e., 30°–50°). Phase lags less than this indicate a dissipation influenced by the anomalous turbulent heat loss to the atmosphere.

The anomalous heat budget and radiation balance gives us additional tools with which to estimate the ocean's climate sensitivity to changing solar irradiance. We observed climate sensitivities ranging over 0.08–0.14°K (W m^{-2})$^{-1}$ from regression conducted on band-passed time sequences in Figure 4, estimated on the basis of changing solar irradiance at the top of the atmosphere. If we compute climate sensitivity on the basis of changing solar insolation, this yields observed estimates of 0.4–0.7°K (W m^{-2})$^{-1}$. From the anomalous heat budget in (2), $T/S_0 = [(\rho C_p H)(K^2 + \sigma^2)^{1/2}]^{-1}$ yields estimates ranging from 0.2 to 0.4°K (W m^{-2})$^{-1}$ for observed estimates of K and H, of the same order as those observed. From the anomalous radiation balance in (3), $\partial T/\partial S = (4\alpha\sigma T^3)^{-1} = 0.3$°K (W m^{-2})$^{-1}$, also of the same order as those observed.

6. Discussions and Conclusions

One important question answered by this study is whether global-average upper ocean temperature responses to changing solar irradiance on decadal and interdecadal scales (i.e., with expected amplitude of 0.05°K) can be detected by surface marine weather and bathythermograph observations collected over the 95 years from 1900 to 1994. The answer is yes, with evidence for this stemming from our ability to observe this upper ocean temperature response in phase over three different ocean basins (i.e., Atlantic, Pacific, Indian), on two different timescales (i.e., decadal and interdecadal), and with two independent data sets (GISST and BT). Moreover, an error analysis was conducted using observed decorrelation scales to assess the numbers of independent estimates in each ocean basin (and over the global ocean), establishing a conservative estimate for the standard error of global-average sea surface temperature anomalies of ±0.01°K. This should not be surprising considering the many millions of observations contained in these data sets.

Associations, phase lags, and climate sensitivities between global-average upper ocean temperature and solar irradiance anomalies derive from the following evidence:

1. Decadal (9–13 years) and interdecadal (18–25 years) periodicities and trends are found to share signals between solar irradiance and sea surface temperature using three different analysis techniques (i.e., power spectra, MSSA, and EOF). Each of these analyses indicates that global-average sea surface temperature anomalies lag or are simultaneous with solar irradiance anomalies, with average phase lags ranging from 30° to 50°.

2. Band-passed-filtered GISST and BT sea surface temperature data sets yield decadal and interdecadal solar-related components in basin and global averages with maximum amplitudes of 0.04° ± 0.01°K and 0.07° ± 0.01°K, respectively. Via regression, these correspond to fluctuations in solar irradiance at the top of atmosphere with maximum amplitudes of approximately 0.5 W m^{-2}, associated with global-average solar inso-

lation of 0.1 W m^{-2} at the sea surface. The former yields the ocean's climate sensitivity of 0.08–0.14°K (W $m^{-2})^{-1}$ to changing solar irradiance at the top of the atmosphere.

3. Solar-related signals in the upper ocean temperature penetrate to 80–160 m depth, which corresponds approximately to the average depth of the main pycnocline over the global ocean. Below these depths, temperature fluctuations become uncorrelated with solar signals, with deeper penetration resisted by the stratification of the main pycnocline. Consequently, the anomalous heat associated with changing solar irradiance is stored in the upper 100 m or so of the ocean, with the heat balances maintained by anomalous heat loss to the atmosphere, not to the deep ocean as suggested by earlier model studies.

Another important question answered by this study is whether the observed 0.04°–0.07°K amplitudes of global-average sea surface temperature anomalies can be explained by the changing solar irradiance at the sea surface (i.e., solar insolation). The answer is yes, with an anomalous heat budget model yielding amplitudes of 0.01°–0.03°K on decadal scales and 0.02°–0.05°K on interdecadal scales that are of the same order as those observed. Uncertainties in this modeling exercise stem from the degree of heat loss to the atmosphere (i.e., related to the phase lag of the upper ocean temperature response to changing solar irradiance) and from the depth of penetration of solar signals in upper ocean temperature. Moreover, this simple model does not contain negative and positive feedbacks with the atmosphere that might alter this quantitative assessment.

We find that observed phase lags between changing solar irradiance and upper ocean temperature response (i.e., 30°–50° on both timescales) are expected from considerations of the radiation balance between solar insolation and long-wave back radiation anomalies. This anomalous balance places an upper limit upon the amplitudes of the global-average sea surface temperature response to changing solar irradiance of approximately 0.03°K (of the same order as that observed), occurring over some equilibration timescale. The latter depends upon the depth to which the solar signal in temperature penetrates into the upper ocean. For penetration depths of 80–160 m observed in this study, back radiation anomalies come into balance with solar insolation anomalies over equilibration timescales of approximately 1.5–3 years, yielding model phase lags of 40°–75° that are similar to those observed. Phase lags less than this indicate a dissipation influenced by the anomalous turbulent heat loss to the atmosphere.

In summary, remarkable consistency exists among observed and model results. Maximum amplitudes of global-average sea surface temperature responses to changing solar irradiance on decadal and interdecadal scales are observed to be 0.04° ± 0.01°K and 0.07° ± 0.01°K, respectively. These amplitudes are of the same order as those derived from the anomalous heat budget (i.e., 0.01°–0.03°K and 0.02°–0.05°K on decadal and interdecadal scales, respectively), taking into consideration observed phase lags and penetration depths. Both of these estimates are of the same order as the 0.03°K response expected from the anomalous radiation balance, the latter also providing an upper limit for phase lags (i.e., 40°–75°) in the anomalous heat budget model that are similar to those observed (i.e., 30°–50°). Furthermore, the ocean's climate sensitivity to changing solar insolation range over 0.4–0.7°K (W $m^{-2})^{-1}$ on decadal and interdecadal scales, of the same order as those estimated from the anomalous heat budget and radiation balance (i.e., 0.2–0.4°K (W $m^{-2})^{-1}$).

The response of upper ocean temperatures to changing solar irradiance is not uniform over the global ocean. Global patterns of decadal and interdecadal sea surface temperature anomalies from GISST and BT data sets are similar to each other, approximately in phase with solar irradiance across the tropical Indian, Pacific, and Atlantic Oceans, but yielding variable phase differences over the extratropical portions of each ocean basin. This relatively uniform tropical phase accounts for the similarity in basin- and global-average sea surface temperature and solar irradiance records observed in Figure 4. As such, global averages from 20°S to 20°N differ little with those computed from 40°S to 60°N, with global-average extratropical sea surface temperature anomalies found to be negligible. This may explain why earlier attempts to observe area-average temperature responses to changing solar irradiance in northern hemisphere extratropics [e.g., *Dettinger et al.*, 1995] achieved ambiguous results.

The fact that these patterns of variability resemble those observed in global ocean-atmosphere coupled models [e.g., *Latif and Barnett*, 1994] strongly suggests that the loss of anomalous heat to the atmosphere (via long-wave back radiation and turbulent air-sea fluxes) in the anomalous upper ocean heat budget may excite these natural modes of ocean-atmosphere coupling or cause them to come into phase with the changing solar insolation. The effect of this hypothetical coupled interaction would be to accentuate the tropical upper ocean temperature response and to diversify the extratropical response to the extent that the latter has little or no global-average expression, as observed. In the future, modeling studies need to be conducted that identify coupling mechanisms responsible for this. Moreover, modelers need to establish whether ocean-atmosphere coupling intensifies (or diminishes) the amplitude of the global-average response to changing solar insolation. Does the atmospheric response provide a net negative or positive feedback?

We have presented here only one mechanism (i.e., solar insolation) for explaining how changing solar irradiance can induce changes in global-average upper ocean temperature. Other mechanisms have been proposed that alter the atmosphere directly and the upper ocean indirectly. One such mechanism has been proposed by *Haigh* [1996], who finds the UV portion of peak solar irradiance increasing ozone production, leading to stratospheric heating and to poleward displacements in the stratospheric and tropospheric wind systems. Another mechanism has been proposed by Svensmark and Friis-Christensen (submitted manuscript, 1996) who find peak solar irradiance decreasing global cloud cover through its influence upon cosmic ray activity and tropospheric ionization. Each of these atmospheric mechanisms has the potential for increasing global-average upper ocean temperatures during peak solar irradiance. In the future, the contributions that these indirect mechanisms make to the response of global-average upper ocean temperatures to changing solar insolation need to be established. Do they intensify or diminish it?

Finally, what do these results on decadal and interdecadal scales have to teach us about the apparent simultaneity of trends observed here in basin- and global-average GISST sea surface temperature anomalies and in reconstructed solar irradiance anomalies? These trends over the past century have

also been observed in the International Panel on Climate Control (IPCC) global surface temperature record (combined land and ocean) by *Lau and Weng* [1995] and in land and sea temperature records examined by *Friis-Christensen and Lassen* [1991] and *Reid* [1991], in each case linearly related to changing solar activity (as observed here). Over the past 500 years, *Lean et al.* [1995a], *Lassen and Friis-Christensen* [1995], and *Crowly and Kim* [1996] have found significant correlations between reconstructed northern hemisphere temperature records and solar irradiance (and activity) records on centennial scales, with regression yielding Earth's climate sensitivity of 0.16°K $(W\ m^{-2})^{-1}$ to changing solar irradiance at the top of the atmosphere. This estimate is similar to centennial climate sensitivities found in solar variability experiments conducted with the GISS general circulation model (GCM) by *Rind and Overpeck* [1993]. Both of these estimates are of the same order as the ocean's climate sensitivity observed in this study (i.e., 0.08–0.14°K $(W\ m^{-2})^{-1}$ on decadal and interdecadal scales. As we learned here, long-wave back radiation can equilibrate upper layer temperature responses to changing solar irradiance after only 1.5–3 years, so we would expect the same on centennial scales as well, perhaps followed by a slow spreading of the temperature response into the deep ocean through both adiabatic and nonadiabatic processes. Therefore, if we apply the ocean's climate sensitivity on these decadal and interdecadal signals to the apparent trend in solar irradiance over the past century, they yield an increase in global-average sea surface temperature of 0.2°–0.3°K in response to the observed rise in solar irradiance of approximately 2.0 W m^{-2} at the top of the atmosphere. This increase is of the same order as that observed (i.e., 0.4°K), suggesting that global warming occurring over the past century was significantly influenced by the corresponding increase in solar irradiance.

Acknowledgments. We extend our appreciation to Russ Davis who provided insight into the global-average anomalous radiation budget and to Ted Walker who conducted many of the statistical analyses contained in this study. This study was supported by the Office of Global Programs at the National Oceanographic and Atmospheric Administration (NOAA), the National Science Foundation (NSF), the Strategic Environmental Research and Development Program (SERDP), the Geological Survey's Global Change Hydrology Program, and the Scripps Institution of Oceanography.

References

Allen, M. R., and L. A. Smith, Investigating the origins and significance of low-frequency modes of climate variability, *Geophys. Res. Lett.*, *21*, 883–886, 1994.

Andersen, N., On the calculation of filter coefficients for maximum entropy spectral analysis, *Geophysics*, *39*, 69–72, 1974.

Auclair, A. N. D., Forest wildlife, atmospheric CO^2, and solar irradiance periodicity (abstract), *Eos Trans. AGU*, *73*(14), Spring Meet. Suppl., 70, 1992.

Cohen, T. J., and E. I. Sweester, The 'spectra' of the solar cycle and of data for Atlantic tropical cyclones, *Nature*, *256*, 295–296, 1979.

Crowley, T. J., and K.-Y. Kim, Comparison of proxy records of climate change and solar forcing, *Geophys. Res. Lett.*, *23*, 359–362, 1996.

Currie, R. G., and O'Brien, Periodic 18.6 year and 10–11-year signals in northeast United States precipitation data, *Int. J. Climatol.*, *8*, 255–281, 1988.

Dettinger, M. D., M. Ghil, and C. L. Keppenne, Interannual and interdecadal variability of United States surface-air temperatures, 1910–1987, *Clim. Change*, *31*, 35–66, 1995.

Folland, D. K., and D. P. Powell, The standard GISST data sets: Version 1 and 2, *Clim. Res. Tech. Note 56*, pp. 50–51, Hadley Cent. for Clim. Predict. and Res., Meteorol. Off., Bracknell, Berkshire, England, 1994.

Foukal, P., and J. Lean, An empirical study of total solar irradiance variation between 1874–1988, *Science*, *247*, 556–558, 1990.

Friis-Christensen, E., and K. Lassen, Length of the solar cycle: An indicator of solar activity closely associated with climate, *Science 254*, 698–700, 1991.

Gandin, L., *Objective Analysis of Meteorological Fields*, translated from Russian, edited by R. Hardin, 242 pp., Ist. Program for Sci. Transl., Jerusalem, 1963.

Gill, A. E., *Atmosphere-Ocean Dynamics*, 662 pp., Academic, San Diego, Calif., 1982.

Granger, C. W. J., *Spectral Analysis of Economic Time Series*, 299 pp., Princeton Univ. Press, Princeton, N. J., 1964.

Haigh, J., The impact of solar variability on climate, *Science*, *272*, 981–984, 1996.

Hoffert, M. I., A Frei, and V. K. Narayanan, Application of solar max ACRIM data to analysis of solar-driven climatic variability on Earth, *Clim. Change*, *13*, 267–285, 1988.

James, I. N., *Introduction to Circulating Atmospheres*, 422 pp., Cambridge Univ. Press, New York, 1994.

Jenkins, G. M., and D. G. Watts, *Spectral Analysis and its Applications*, 525 pp., Holden-Day, Merrifield, Va., 1968.

Kaylor, R. E., Filtering and decimation of digital time series, *Tech. Note BN 850*, Inst. for Phys. Sci. and Technol., Univ. of Md., College Park, 1977.

Lassen, K., and E. Friis-Christensen, Variability of the solar cycle length during the past five centuries and the apparent association with terrestrial climate, *J. Atmos. Terr. Phys.*, *57*, 835–845, 1995.

Latif, M., and T. P. Barnett, Causes of decadal climate variability over the North Pacific and North America, *Science*, *266*, 634–637, 1994.

Lau, K.-M., and H. Weng, Climate signal detection using wavelet transform: How to make a time series sing, *Bull. Am. Meteorol. Soc.*, *76*, 2391–2402, 1995.

Lean, J. L., J. Beer, and R. Bradely, Reconstruction of solar irradiance since 1610: Implications for climate change, *Geophys. Res. Lett.*, *22*, 3195–3198, 1995a.

Lean, J. L., O. R. White, and A. Skumanich, On the solar ultraviolet irradiance during the Maunder Minimum, *Global Biogeochem. Cycles*, *9*, 171–182, 1995b.

Mann, M. E., and J. Park, Global-scale modes of surface temperature variability on interannual to century timescales, *J. Geophys. Res.*, *99*, 25,819–25,833, 1994.

Mitchell, J. M., C. W. Stockton, and D. M. Meko, Evidence of a 22-year rhythm of drought in the western United States related to the Hale solar cycle since the 17th century, in *Solar Terrestrial Influence on Weather and Climate*, edited by B. M. McCormac and T. A. Seliga, pp. 124–144, D. Reidel, Norwell, Mass., 1979.

Newell, N. E., R. E. Newell, J. Hsuing, and W. Zhongxiang, Global marine temperature variation and the solar magnetic cycle, *Geophys. Res. Lett.*, *16*, 311–314, 1989.

Parker, D. E., P. D. Jones, C. K. Folland, and A. Bevan, Interdecadal changes of surface temperature since the late nineteenth century, *J. Geophys. Res.*, *99*, 14,373–14,399, 1994.

Perry, C. A., Solar-irradiance variations and regional precipitation fluctuations in the western USA, *Int. J. Climatol.*, *14*, 969–983, 1994.

Preisendorfer, R. W., *Principal Component Analysis in Meteorology and Oceanography*, 425 pp., Elsevier, New York, 1988.

Reid, G. C., Solar total irradiance variations and the global sea surface temperature record, *J. Geophys. Res.*, *96*, 2835–2844, 1991.

Rind, D., and J. Overpeck, Hypothesized causes of decade-to-century climate variability: Climate model results, *Quat. Sci. Rev.*, *12*, 357–374, 1993.

Robinson, M. K., Atlas of North Pacific Ocean monthly mean temperature and mean salinities of the surface layer, *Nav. Oceanogr. Ref. Publ.*, *2*, Nav. Res. Lab., Bay St. Louis, Miss., 1976.

Robinson, M. K., R. Bauer, and E. Schroeder, Atlas of North Atlantic-Indian Ocean monthly mean temperature and mean salinities of the surface layer, *Nav. Oceangr. Ref. Publ.*, *18*, Nav. Res. Lab., Bay St. Louis, Miss., 1979.

Seleshi, Y., G. R. Demaree, and J. W. Delleur, Sunspot numbers as a possible indicator of annual rainfall at Addis Ababa, Ethiopia, *Int. J. Climatol.*, *14*, 911–923, 1994.

Snedecor, G. W., and W. G. Cochran, *Statistical Methods*, 507 pp., Iowa State Univ. Press, Ames, 1980.

Vautard, R., P. Yiou, and M. Ghil, Singular-spectrum analysis: A toolkit for short, noisy, chaotic signals, *Physica D*, *58*, 95–126, 1992.

White, W. B., Design of a global observing system for basin-scale upper ocean temperature anomalies, *Prog. Oceanogr.*, *36*, 169–217, 1995.

Wigley, T. M. L., and S. C. B. Raper, Climate change due to solar irradiance changes, *Geophys. Res. Lett.*, *17*, 2169–2172, 1990.

Wilson, R. C., and H. S. Hudson, A solar cycle of measured and modeled solar irradiance, *Nature*, *351*, 42–44, 1991.

Young, H. D., *Statistical Treatment of Experimental Data*, 172 pp., McGraw-Hill, New York, 1962.

D. R. Cayan and W. B. White, Scripps Institution of Oceanography, University of California at San Diego, 9500 Gilman Dr., La Jolla, CA 92093-0230. (e-mail: dcayan@ucsd.edu; wbwhite@uscd.edu)

M. D. Dettinger, U. S. Geological Survey, 5735 Kearny Villa Rd., San Diego, CA 92123. (e-mail: mddettin@usgs.gov)

J. Lean, Naval Research Laboratory, 4555 Outlook Ave., S. W., Washington, D. C. 20375. (e-mail: lean@dememter.nrl.navy.mil)

(Received May 22, 1996; revised October 2, 1996;
accepted October 8, 1996.)